ELSEVIER

Journal of Biomechanics 40 (2007) 1350–1361

JOURNAL OF BIOMECHANICS

www.elsevier.com/locate/jbiomech
www.JBiomech.com

Virtual musculo-skeletal model for the biomechanical analysis of the upper limb

E. Pennestrì, R. Stefanelli, P.P. Valentini, L. Vita*

Department of Mechanical Engineering, University of Rome Tor Vergata, Via del Politecnico, 1–00133 Rome, Italy

Accepted 12 May 2006

Abstract

In this paper, a musculo-skeletal model of the upper limb is presented. The limb is modelled as a three-dimensional 7 degrees-of-freedom system, linked to the shoulder, which has been considered as frame. The upper limb model is made up of four links corresponding to the most important body segments: the humerus, the ulna, the radius and the hand, considered as a single rigid body. Particular attention has been paid to the modelling of joints in order to mimic all the possible arm and forearm movements (including prono-supination). The model also includes 24 muscles. The mathematical model used to describe the muscles is that proposed by Zajac in 1989, modified by the authors. The kinematic analysis has been performed including an ergonomics index to take into account the posture and joint physical limits. Moreover an optimization criterion based on minimum activation pattern has been included in order to find muscular activation coefficients. The results of the proposed methodology concerning muscular activations have been compared to those coming from processed EMG signals, which have been acquired during experimental tests.

Keywords: Upper limb; Muscles; Ergonomics; Disabled people

1. Introduction

In many mechanical fields the interaction between man and machine has to be studied in depth in order to improve human performances and ensure safety in every working condition. Moreover in special applications for disabled people, the human–machine interface has to be designed taking into account ergonomics and fewer abilities. For this reason mathematical models can be built up in order to simulate these interactions and test several changes in a virtual way, saving money and time. The detail of these models depends on the parameters that need to be investigated and on the accuracy required. In many cases a simplified description of body shapes and joints is sufficient to reproduce gross motion and general operation (Valentini and Vita, 2003). For more accurate studies, detailed models are required (Silva, 2004). Moreover a comprehensive model requires many parameters to be correctly defined and very complex mathematics, which may lead to equations difficult to be solved or requiring an unacceptable solution time.

Ergonomic study about man and machine interaction often implies the knowledge of muscular forces and the estimation of body segments attitude during operations (Allard et al., 1995). Multibody dynamics approach reveals as a powerful instrument to simulate kinematics of body links. In order to mimic the dynamical behaviour, muscles have to be introduced in the multibody equations. For a single movement, there are many muscles, which activate simultaneously and interact together. This kind of problem may have multiple solutions. In order to find a physically

*Corresponding author. Tel.: +39 0672597136; fax: +39 062021351.
E-mail addresses: valentini@ing.uniroma2.it (P.P. Valentini), vita@ing.uniroma2.it (L. Vita).

0021-9290/$ - see front matter © 2006 Elsevier Ltd. All rights reserved.
doi:10.1016/j.jbiomech.2006.05.013

acceptable solution, the problem can be interpreted as an optimization problem. The objective functions to be minimized can be built taking into account ergonomic factors. Many authors (Murray et al., 2000; Zajac, 1989; Kole et al., 1996; Van der Helm and Veeger, 1996) investigated these aspects. A unique criterion is longer to be found and several approaches can be used alternatively (Rehbinder and Martin, 2001).

The proposed model has been developed during a research project, which had the target of the study and the optimization of automotive cockpits for less able people. Italian standards require some initial tests in order to assess the capability and residual forces of these subjects. After passing these tests performed on an instrumented driving simulator, one can obtain a special driving licence. For this reason multibody techniques have been considered as a powerful instruments to develop a mathematical model to be used together with data coming from experimental campaigns in order to reproduce the muscular activity and joint reactions during driving and to test virtually several changes in the cockpit design.

2. Upper limb kinematics

2.1. Joint modelling

In order to reproduce the correct kinematics of upper limb the first step is to investigate the actual joints of human arm (Kapandji, 1996). The upper limb can be viewed as a biomechanical system (Fig. 1) made up of four rigid links, which are the main body segments: humerus, radius, ulna, hand.

These links are connected together by means of the following joints:

- Shoulder joint which connects the humerus with the shoulder;
- Elbow joint which connects the humerus with both radius and ulna;
- Wrist joint, which connects the radius with the ulna and the radius with the hand.

Before deducing the equations of kinematics some important anatomical considerations have to be made (Veeger et al., 1997). First of all we have to define the mechanical axis and the anatomical axis of bones. Let us consider the humerus depicted in Fig. 2. The mechanical axis is the axis along which the forces are transmitted while the anatomical axis is the physical bone axis. The difference between them is about few degrees. In the proposed model the reference x-axis of each link has been assumed to be the mechanical axis. Let us now investigate each joint in depth.

Considering the simulation we are going to perform, in which almost no movement is expected in the shoulder joint, the complex shoulder joint may be modelled as an ideal spherical joint.

Modelling the elbow joint is more complex (Fig. 2). At elbow a spherical end of radius comes into contact with a cavity in the humerus lower end. At the same end the humerus contacts with a cylindrical surface of the ulna too. Thus the elbow joint can be modelled as a spherical joint between humerus and radius and a revolute joint between the humerus and the ulna. The axis of the revolute joint passes through the centre of the spherical one. Actually, during prono-supination

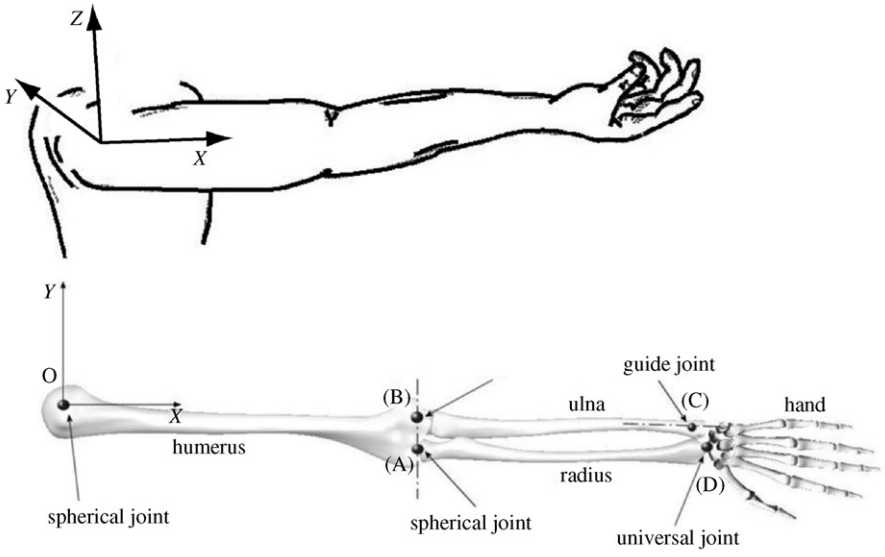

Fig. 1. Upper limb reference posture, nomenclature and joint location.

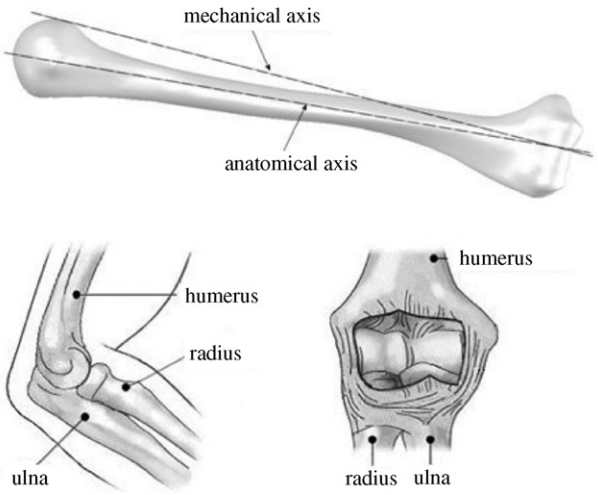

Fig. 2. Anatomical and mechanical axes and elbow joint detail.

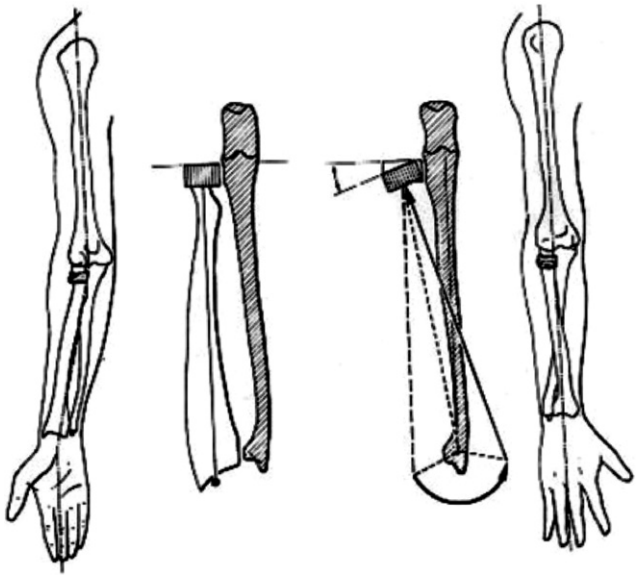

Fig. 3. Prono-supination movement.

(Fig. 3) the ulna is not fixed with respect to the humerus, but performs a small swaying (lateral) motion as well as a small axial sliding along its axis with respect to the humerus bone (Kapandji, 1996). Some authors propose to take into account this behaviour using a kineto-elastic model (Kecskeméthy and Weinberg, 2005). For the investigation of the present work (i.e. simulation of a less able people during driving) the angle describing prono-supination is limited within a small range, thus this swaying behaviour has been neglected.

At the other extremity both radius and ulna are connected with ligaments, which keep them adjacent. The joint constrains the mechanical axis of the ulna to pass through the *C* point of the radius (Fig. 1). This very complex joint can be modelled using a guide between the *C* point and the ulna axis. This joint together with elbow joint allows the movement of pronosupination, which is described in Fig. 3.

The other wrist joint represents the connection between the radius and the hand. This joint can be modelled as a universal joint, which does not permit three translations and one rotation (along radius mechanical axis). In the actual wrist joint the axes of two rotations are not incident, but it seems to be a valid and useful approximation. Note that no connection occurs between ulna and hand (Zatsiorsky, 1995).

We can summarize all the investigated joints as (see Figs. 1 and 4)

- Spherical joint at *O* between the frame (or the rest of the body) and humerus (3 constraint equations);
- Revolute joint at *B* between humerus and ulna (5 constraint equations);
- Spherical joint at *A* between humerus and radius (3 constraint equations);
- Guide at *C* between ulna and radius (2 constraint equations);
- Universal joint at *D* between radius and hand (4 constraint equations).

In the model there are 17 constraint equations and 24 (4 bodies with 6 degrees-of-freedom each) generalized coordinates, which leads to 7 degrees-of-freedom.

Let us now introduce some driving constrains. They can be added to joint equations in order to describe the desired movement of the hand. In the proposed simulation we constrained the hand to grab a knob on a steering wheel. This device is often mounted on some vehicles for disabled people. This assumption will not affect or limit the capabilities of the model. Driving constraints can be added, deleted or changed in order to describe different hand trajectories and different movements. The kinematics and dynamics described in the following sections are independent from the number or the kind of these driving constraints.

The assumption about the hand, which grabs the steering knob, introduces other 5 constraint equations leaving free only the rotation about the knob axis. The other degree-of-freedom still active refers to the motion of the whole arm during the steering operation. The position and the attitude of the hand are prescribed by steer geometry and inclination.

Thus there are not enough equations to solve the kinematics of the system. We have to introduce some objective functions in order to find a solution, which satisfies the constraint equations and minimize these functions.

For this reason the authors implemented an ergonomic function, which will be explained in the next section. It is important to observe that this function is suitable for every analysis and for every chosen driving

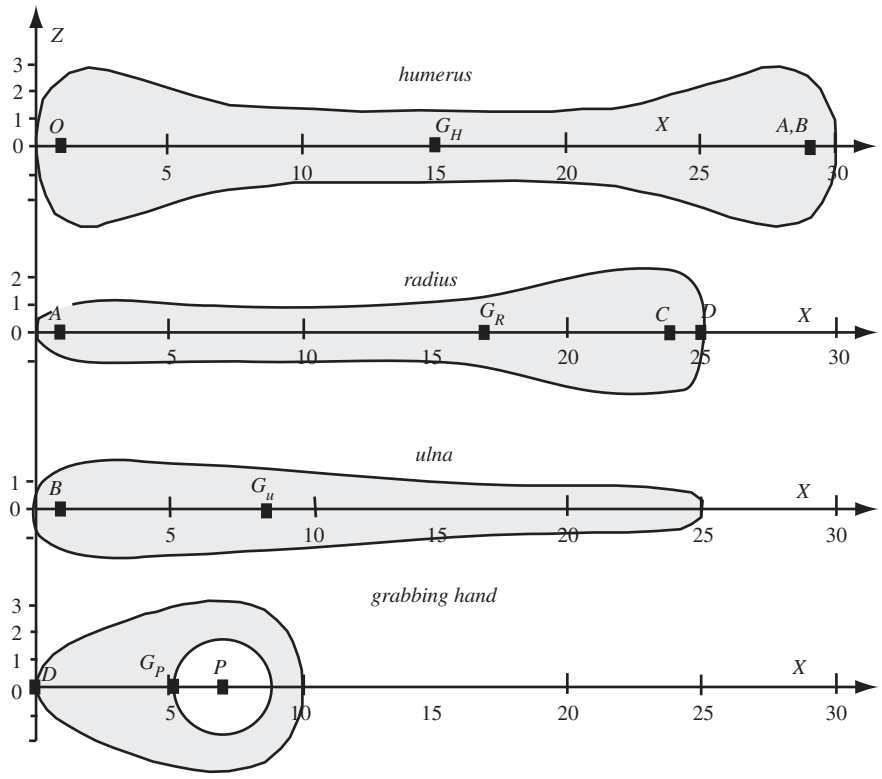

Fig. 4. Segment reference axis and points.

constraint (not only for the investigated operation), because it allows to solve the system with more unknowns than equations.

2.2. Ergonomic index

Every human joint has physical limits, which reduce the range of motion of the links. We can model these limits for each joint according to anatomical properties (Zatsiorsky, 1995). Let us define the angles α_i ($i = 1, 2, \ldots, 9$) as follow (see Fig. 1 for axis definition):

- α_1 as the angle of the humerus w.r.t. global Y-axis;
- α_2 as the angle of the humerus w.r.t. global Z-axis;
- α_3 as the angle of the humerus w.r.t. global X-axis;
- α_4 as the relative angle between humerus and ulna (about humerus y-axis);
- α_5 as the relative angle between radius and humerus (about humerus y-axis);
- α_6 as the relative angle between radius and humerus (about humerus z-axis);
- α_7 as the relative angle between radius and humerus (about humerus x-axis);
- α_8 as the relative angle between hand and radius (about radius y-axis);
- α_9 as the relative angle between hand and radius (about radius z-axis).

Table 1
Limits for joint angles (the reference position is depicted in Fig. 1)

Angle	Min value (deg) (α_{min})	Max value (deg) (α_{max})
α_1	−90	135
α_2	−80	45
α_3	−100	25
α_4	−140	0
α_5	−140	0
α_6	0	15
α_7	−180	0
α_8	−80	80
α_9	−25	50

Table 1 summarizes the maximum and minimum values for these angles for a male subject. Note that the limits depend on the physical condition of the investigated subject. Moreover the angles are not independent. In fact α_5 and α_6 depend on α_4 and α_7 because of the pronosupination joints.

We can define the ergonomic function $H(\alpha_i, i = 1, \ldots, 9)$ as

$$H(\alpha) = \sum_i w_i \frac{(\alpha_i - \alpha_{Mi})^4}{(\Delta\alpha_i)^4}, \quad (1)$$

where α_i are the joint angles, w_i are the weighting coefficients

$$\alpha_{Mi} = \frac{\alpha_{max} + \alpha_{min}}{2} \text{ and } \Delta\alpha_i = \frac{\alpha_{max} - \alpha_{min}}{2}.$$

It is herein assumed that the more ergonomic solutions are reached when the function in (1) is minimized. Physically it means that a movement could be judged comfortable when the joint does not reach its limits. The more the joints are far from their limits of movement, the more the configuration is ergonomically correct. The overall function in (1) is the sum of ergonomic functions of each joint weighted with proper coefficients. In general rotation about local x-axes are less comfortable than those about local y- and z-axes. An example of this concept comes from the wrestling where many attempts of immobilizing the opponent concern forced movement of arm with a rotation about the longitudinal x-axis. Weighting coefficients can be chosen according to experimental physiological tests. People with disabilities may suffer pain when reaching some positions. In these cases the coefficients may prevent such harmful movements. Standard values for the weighting coefficients are: 0.7 for α_1, α_3, α_4, α_5, 0.8 for α_2, α_6, α_9 and 1.0 for α_7, α_8. The reference position shown in Fig. 1 is not the most comfortable position because of closeness of physiological limits for prono-supination and flexion movements.

2.3. Kinematics equations

The constraint equations $\{\Phi(q,t)\}$ describing the physical joints and driving constraints are 22. The generalized coordinates $\{q\}$ are 24. In order to solve the optimization problem we have to introduce a Lagrangian function L as

$$L = H(\alpha) + \{\lambda\}^{\mathrm{T}}\{\Phi(q,t)\}. \tag{2}$$

This function is a sum of the ergonomic function and the dot product between Lagrange multipliers and the constraints vector. The derivative of Eq. (2) w.r.t. the variables $\{\lambda\}$ and $\{q\}$, can be computed as

$$\frac{\partial L}{\partial \lambda_i} = \{\Phi(q,t)\},$$
$$\frac{\partial L}{\partial q_i} = \frac{\partial H}{\partial \alpha_j}\frac{\partial \alpha_j}{\partial q_i} + \frac{\partial(\{\lambda\}^{\mathrm{T}}\{\Phi(q,t)\})}{\partial q_i}. \tag{3}$$

These equations have to be set equal to 0 in order to find the solution, which minimizes the H function satisfying the constraints $\{\Phi(q,t)\}$, leading to

$$\{\Phi(q,t)\} = 0,$$
$$\frac{\partial H}{\partial \alpha_j}\frac{\partial \alpha_j}{\partial q_i} + [\Phi_q]^{\mathrm{T}}\{\lambda\} = 0. \tag{4}$$

The $\partial H/\partial\alpha_j$ term can be computed from Eq. (1). The $\partial\alpha_j/\partial q_i$ term can be deduced expressing the functions $\alpha_j = f(q_i)$ using transformation matrices between relative reference frames (where α_j are defined) and non-moving frame (where q_i are defined).

The Eq. (4) is a system of 46 nonlinear equations (22 + 24) and 46 unknowns (24 generalized coordinates and 22 Lagrange multipliers). It can be solved, finding the variables describing each link position over time. Velocities and accelerations can be computed by differentiation w.r.t. time of position functions.

3. Muscle modelling

3.1. Forces exerted by muscles

A generic muscle can be viewed as a set of fibres, which connect two tendons. These fibres can exert a force by contracting (Zajac, 1989). The maximum force which can be exerted by a muscle depends on the physiological cross section area (pCSA) (Epstein and Hertzog, 1998; Garner and Pandy, 2003) which depends on muscular mass (M_{m}), the pinnation angle (β), muscle length (L_{m}) and density (ρ):

$$\mathrm{pCSA} = \frac{M_{\mathrm{m}}\cos\beta}{L_{\mathrm{m}}\rho}. \tag{5}$$

The maximum normal pressure which can effort a muscle is within the range of 0.2–0.35 N/mm^2. The maximum force F_0 can be obtained multiplying this pressure by pCSA.

Literature presents many mathematical models apt to describe the dynamic activation and the contraction of a muscle. Maxwell, Voight and Kelvin models only describe the passive action, while Hill model (1938) includes also the active force on contraction. According to the authors a suitable model to be included into multibody system is those proposed by Zajac (1989). According to this model the muscular force F_{m} is a sum of active component F_{a} and passive component F_{p} as

$$F_{\mathrm{m}} = F_{\mathrm{a}} + F_{\mathrm{p}} = F_0(f_1 f_2 a(t) + f_3), \tag{6}$$

where $a(t)$ is the activation function which assumes a value within the range 0–1 (0 for not-activated muscle, 1 for fully activated muscle) while the functions f are complex and they depend on other sub functions. They can be well approximated improving computational performances (as concern both time and accuracy) as simpler functions depending on stretching, contraction velocity and voluntary activation coefficient:

$$f_1 = \mathrm{e}^{[-40(x-0.95)^4+(x-0.95)^2]},$$
$$f_2 = 1.6 - 1.6\,\mathrm{e}^{[-1.1/(-v+1)^4+0.1/(-v+1)^2]},$$
$$f_3 = 1.3\cdot\arctan[0.1(x-0.22)^{10}],$$
$$x = \frac{l}{l_0} \quad \text{and} \quad v = \frac{V}{2.5}. \tag{7}$$

The functions f_1 and f_3 depend on muscle length l, while f_2 depends on muscular contraction velocity V. The variable l_0 is the muscle length before activation including the length of the tendons. Under this

assumption the tendons are sufficiently stiff with respect to the muscles so that the change in their length is negligible compared to a change in muscles length (Garner and Pandy, 2003).

3.2. Muscles in upper limb

In the proposed model the upper limb has 24 muscles (see Fig. 6 for details). For each muscle the following parameters have to be correctly defined:

- l_0 length (muscle + tendons);
- F_0 peak isometric force;
- connecting point to the first bone (3 coordinates);
- connecting point to the second bone (3 coordinates).

These parameters have been carried out from a database proposed by Yamaguchi (Yamaguchi, 2001) and summarized in Table 2.

A generic muscle can be introduced into a multibody model in the same way we can include a spring-actuator element (Rasmussen et al., 2005a, b): with an action-reaction force which acts along connection line.

Considering a muscle i which acts on a body k, the generalized muscular force can be computed from (6) as

$$\{F^k_{\mathrm{m}\_i}\} = \{W^k_i(q,\dot{q})\}a_i(t) + \{F^k_{\mathrm{pass}\_i}(q)\}, \tag{8}$$

where $\{W^k_i\}$ collects the actions of active forces and the corresponding torques, while $\{F^k_{\mathrm{pass}\_i}\}$ collects the actions of passive forces and the corresponding torques. Both of them can be computed using principle of virtual

Table 2
Properties of muscles and anchor points

Muscle	Name	L_0 (mm)	F_0 (N)	1st link attach point (mm)			2nd link attach point (mm)		
				x	y	z	x	y	z
Muscles connecting humerus to rest of the body									
1	Coracobrachialis	200	63	20	30	35	174	21	0
2	Deltoid	170	240	−30	40	15	106	−24	−11
3	Latissimus dorsi	135	360	−35	90	−125	0	0	−13
4	Pectoralis major	190	210	45	95	−125	17	−13	0
5	Supraspinatus	90	98	−20	90	35	−14	17	27
6	Infraspinatus	105	210	−15	80	−40	28	−19	27
7	Trapezius	100	240	0	80	10	31	0	24
8bis	Biceps brachii	230	47	0	−15	10	252	21	0
Muscles connecting radius to rest of the body									
10bis	Triceps brachii	285	135	−25	20	−20	38	27	−20
Muscles connecting ulna to rest of the body									
8	Biceps brachii	270	90	0	−15	10	38	0	10
Muscles connecting humerus to ulna									
9	Anconeus	75	40	265	5	−19	42	12	29
10	Triceps brachii	210	108	78	11	−10	38	−27	−15
Muscles connecting humerus to radius									
11	Brachialis	105	167	176	−8	16	33	5	10
12	Brachioradialis	220	45	246	−27	0	238	−12	0
13	Pronator teres	70	54	220	33	−5	55	−11	24
Muscles connecting humerus to hand									
14	Cubitalis anterior	255	35	149	24	5	6	27	7
15	Flexor carpi ulnaris	255	51	249	27	0	5	30	7
16	Extensor carpi ulnaris	210	42	249	27	0	5	30	−7
17	Extensor digitorum	225	46	242	20	−20	38	0	−10
19	Flexor digitorum sup.	220	45	227	11	21	5	−18	−6
20	Flexor carpi radialis	235	72	249	27	0	3	12	5
Muscles connecting ulna to radius									
18	Pronator quadrus	45	78	200	12	9	236	−5	12
21	Supinator brevis	50	30	−13	−27	−12	28	10	−10
Muscles connecting ulna to hand									
22	Abductor digiti V	140	36	115	−15	−5	10	−18	−7

Note that muscle number 8 and 10 have three points of connection on different bones, thus they have been considered as 4 muscles (8, 10, 8 bis and 10 bis). The attachment point coordinates refer to systems in Fig. 4.

work. The force due to spring-actuator force element can be modelled similarly.

Thus the overall generalized force acting on kth link can be computed as

$$\{F^k_{\mathrm{m}}\} = \sum_i \{F^k_{\mathrm{m\_}i}\} = \sum_i \{W^k_i(q,\dot{q})\}a_i(t) + \{F^k_{\mathrm{pass\_}i}(q)\}. \tag{9}$$

Considering all the bodies in the system the generalized forces coming from the muscles can be written as

$$\{F_{\mathrm{m}}\} = [W(q,\dot{q})]\{a(t)\} + \{F_{\mathrm{pas}}\}. \tag{10}$$

4. Upper limb inverse dynamics

The purpose of the model is the estimation of muscular activations and joint reactions (Pigeon et al., 1996). The equations of dynamics for a complete upper limb system can be written as

$$[M]\{\ddot{q}\} + [\Phi_q]^{\mathrm{T}}\{\lambda\} = [W]\{a\} + \{F_{\mathrm{pas}}\} + \{F_{\mathrm{ext}}\}, \tag{11}$$

where $[M]$ is the global mass matrix, $\{q\}$ the vector of generalized coordinates, $[\Phi_q]$ the Jacobian matrix of constraint equations $\{\Phi\}$ w.r.t. generalized coordinates, $\{\lambda\}$ the vector of constraint Lagrange multipliers, $[W]$ the muscular activation matrix, $\{a\}$ the vector of activation coefficients, $\{F_{\mathrm{pas}}\}$ the vector of muscular passive forces, $\{F_{\mathrm{ext}}\}$ the vector of external forces (such as gravity).

The target of inverse dynamics is the computation of vectors $\{\lambda\}$ and $\{a\}$ starting from the knowledge of the kinematic features of the system in terms of generalized coordinates. The vector $\{q\}$ can be computed solving the kinematics Eq. (4). The system (11) can be rearranged into:

$$[\Phi_q]^{\mathrm{T}}\{\lambda\} - [W]\{a\} = \{F_{\mathrm{pas}}\} + \{F_{\mathrm{ext}}\} - [M]\{\ddot{q}\}. \tag{12}$$

The system in (12) is made of 24 equations and 46 unknowns (22 Lagrange multipliers and 24 muscular activity coefficients). In order to get a solution we have to define the muscular activations rate Mu as

$$\mathrm{Mu} = \sum_i \frac{a_i^2}{2}. \tag{13}$$

This function describes how the muscles of the system are active.

The system in (12) can be written in a compact form collecting all the unknown variables as

$$[A]\{x\} = \{f\}, \tag{14}$$

where

$$[A] = \begin{bmatrix}[\Phi_q]^{\mathrm{T}} & [W]\end{bmatrix}, \{x\} = \{\{\lambda\} \quad \{a\}\}^{\mathrm{T}}$$

and

$$\{f\} = -\{F_{\mathrm{pas}}\} - \{F_{\mathrm{ext}}\} - [M]\{\ddot{q}\}.$$

In order to solve Eq. (14) we can define another Lagrange function L_{m}, which has to be optimized:

$$L_{\mathrm{m}} = \mathrm{Mu} + \{\chi\}^{\mathrm{T}}([A]\{x\} - \{f\}). \tag{15}$$

The derivatives of (15) w.r.t variable $\{x\}$ and multipliers $\{\chi\}$ leads to

$$\begin{aligned}&\frac{\partial L_{\mathrm{m}}}{\partial \chi_i} = 0 \rightarrow [A]\{x\} - \{f\} = 0,\\ &\frac{\partial L_{\mathrm{m}}}{\partial x_i} = 0 \rightarrow \frac{\partial \mathrm{Mu}}{\partial x_i} + \frac{\partial\left(\{\chi\}^{\mathrm{T}}[A]\{x\}\right)}{\partial x_i} = 0.\end{aligned} \tag{16}$$

The system in (16) can be rearranged after some algebraic computation to obtain a more compact expression:

$$\begin{bmatrix}[I_A]_{46\times 46} & [A]^{\mathrm{T}}_{46\times 24}\\ [A]_{24\times 46} & [0]_{24\times 24}\end{bmatrix}\begin{Bmatrix}x_{46}\\ \chi_{24}\end{Bmatrix} = \begin{Bmatrix}0_{46}\\ f_{24}\end{Bmatrix}, \tag{17}$$

where $[I_A] = \begin{bmatrix}[0]_{22\times 22} & [0]_{22\times 24}\\ [0]_{24\times 22} & [I]_{24\times 24}\end{bmatrix}$ and $[I]$ is the identity matrix.

The equations in (17) can now be solved for unknown variables. The vector of solution has all the activation coefficients $\{a\}$ greater or equal to 0 and lower than 1 in order to represent a physically acceptable solution. It is very common that the first solution contains negative or higher than one value. It means that the minimum of the function cannot be assumed as a physically consistent condition. For this reason the actual (physically acceptable) solution can be obtained by iterations using the following algorithm:

1. Let us first assume that the solution of optimization is $\{y_{\mathrm{s}}\}$, which contains unacceptable activation coefficients. In this case we can define another vector $\{y_{\mathrm{p}}\} = \{x_{\mathrm{p}} \quad \chi_{\mathrm{p}}\}^{\mathrm{T}}$ as

$$\begin{aligned}&\text{if } 23 \leqslant i \leqslant 46 \quad y_{\mathrm{p\_}i} = \begin{cases} y_{\mathrm{s\_}i} - \varepsilon & \text{if } y_{\mathrm{s\_}i} > 1,\\ y_{\mathrm{s\_}i} & \text{if } 0 \leqslant y_{\mathrm{s\_}i} \leqslant 1,\\ y_{\mathrm{s\_}i} + \varepsilon & \text{if } y_{\mathrm{s\_}i} < 0\end{cases}\\ &\text{else} \qquad\qquad y_{\mathrm{p\_}i} = y_{\mathrm{s\_}i},\end{aligned} \tag{18}$$

   where ε is the correction coefficient and the subscript$_{_i}$ represents the ith element of the vector.
2. Then we can compute the vector of residues as

$$\{r\} = [A]\{x_{\mathrm{p}}\} - \{f\}. \tag{19}$$

3. We can now solve the following system for $\{\mathrm{d}y\} = \{\mathrm{d}x \quad \mathrm{d}\chi\}^{\mathrm{T}}$:

$$\begin{bmatrix}[I_A] & [A]^{\mathrm{T}}\\ [A] & [0]\end{bmatrix}\begin{Bmatrix}\mathrm{d}x\\ \mathrm{d}\chi\end{Bmatrix} = \begin{Bmatrix}0\\ r\end{Bmatrix}. \tag{20}$$

4. A new solution vector can be computed as $\{y_n\} = \{y_p\} - \{dy\}$. It can be deduced that this vector satisfy the following equations :

$$\begin{bmatrix} [I_A] & [A]^T \\ [A] & [0] \end{bmatrix} \{y_n\} = \begin{Bmatrix} d\chi \\ f \end{Bmatrix}. \quad (21)$$

This system implies the following equations to be satisfied:

$$[A]\{x_n\} = \{f\}, \quad (22)$$

which means that the new solution is a solution of the previous system (14) . The new global solution is no more a Lagrange function minimum but it still satisfies the equilibrium condition (14).

5. The iteration continues until the norm of residues vector is smaller than a chosen tolerance and the activation coefficients are within the 0–1 range.

5. Simulation results and experimental tests

The proposed multibody model has been used for the analysis of steering wheel turning operation of a less able person on a car-driving simulator. This device is composed by a car interior, fixed to a table and equipped with an optical angular encoder to measure the angular displacement of the steering wheel shaft (see Fig. 5). Positioning error is estimated within the range $\pm 0.5^\circ$. The seat and the dashboard can be adjusted to different positions. The purpose of this test is to understand how the upper limb behaves during steering operation and which are the muscles mainly involved in this movement. The simulation observes an upper limb whose hand grabs a steering wheel knob. The input parameter is the angular displacement of the steering wheel, which has been monitored experimentally (see Fig. 6).

Fig. 5. Experimental setup for acquiring EMG signals.

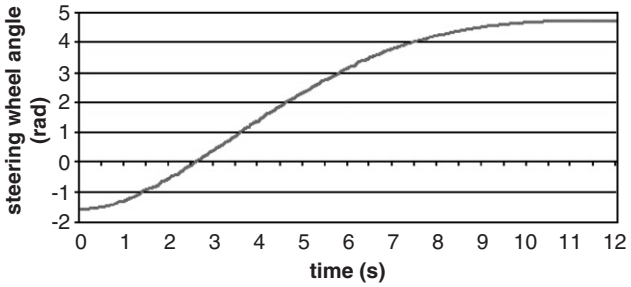

Fig. 6. Measured angular displacement of steering wheel.

The geometrical and mass properties of the body segments have been set according to the values listed in Tables 3 and 4, respectively.

The plots of the computed reaction forces and torques vs. time are reported in Fig. 7 where they are collected by joints. It should be observed that the peak force values arise when the steering wheel angular displacement is about $\pi/2$ ($t = 4$ s, the hand is in the up right position). In this position the shoulder muscles (i.e. the trapezius and sopraspinatus) exert the maximum force by activation of about 20–25% (Fig. 8). As a consequence, the shoulder joint exerts also the highest reaction forces. Since this position is near to physiological limits, the wrist joint undergoes also the highest reaction forces. Several muscles are activated together during the movement. It can be observed that at the end of a muscle activation (i.e. when activation coefficient decreases to zero) and the body segment reduce its velocity, the antagonist muscle is always activated in order to control the braking action. The activation of the antagonist is always lower than the protagonist one (about 10%) and it is proportionally dependent on the deceleration of body segment.

Computationally, the proposed methodology does not require any special hardware resource. The algorithm to find muscular activations, which is a key procedure, converges after about 50 iterations starting from a null vector of initial guesses. Using guess values from the previous step, the number of iterations is sensibly reduced.

The results obtained from simulation have been compared to those from experimental EMG tests. With reference to Fig. 5, the subject test has been monitored using an EMG signal acquisition system. Three muscles have been monitored using two electrodes each: the biceps brachii (muscle no. 8 in Table 2), the triceps brachii (no. 10) and the flexor carpi ulnaris (no. 15). The steering movement has been repeated 5 times and mean signal values have been computed. After the tests the muscular activity signals have been filtered with a low-pass filter (Yamazaki et al., 1995) in order to smooth them and they have been rescaled to the maximum isometric peak according to (Tal'Nov et al., 1999).

Table 3
Geometry properties of bones and joints

Point	Body	Point coordinates w.r.t. body centre of mass reference frame		
		x	y	z
O	Fixed body	0	0	0
	Humerus	$-d_h$	0	0
A	Humerus	e_h	$-b_h/2$	0
	Radius	$-d_r$	0	0
B	Humerus	e_h	$b_h/2$	0
	Ulna	$-d_u$	0	0
C	Radius	c_r	b_h	0
D	Radius	e_r	0	0
P	Hand	$-d_p$	0	0
	Hand	e_p	0	0

Parameter	Value (mm)
$-d_h$	140
e_h	140
b_h	32
$-d_r$	159
e_r	81
c_r	71
$-d_u$	78
$-d_p$	51
e_p	19

Table 4
Mass and inertial properties of body segments

Property	Humerus	Radius	Ulna	Hand (grabbing)
Actual mass (including muscles) (kg)	1.89	0.498	0.752	0.81
Actual moment of inertia w.r.t. local x axis (kg mm^2)	1890	540	300	2200
Actual moment of inertia w.r.t. local y axis (kg mm^2)	14,592	3122	4170	3769
Actual moment of inertia w.r.t. local z axis (kg mm^2)	14,592	3122	4170	3769

Note that in order to simulate the muscular mass of the upper limb segment, inertial properties have been multiplied by an apparent mass density, thus the value of mass and moments of inertia does not refer only to the bone but they include also muscle and tendon mass.

Figs. 9 and 10 reports a comparison between numerical and experimental results concerning biceps and triceps activation coefficients.

It can be observed that both the simulated and measured activation peaks appear almost simultaneously. This means that the model seems to mimic a correct muscular activation pattern with the same activation sequence. On the other hand, the experimentally measured activation coefficients have sharper peaks than the simulated ones. This can be explained considering that the optimization algorithm, which is based on several iterations, smooths and regularizes the activation coefficients. This is not a limit because the max error value on activations is bounded within 5% for the biceps, 10% for the triceps. Similar results have been obtained for the flexor for which the error in maximum activation error is 7%.

6. Conclusions

In this paper a detailed upper limb virtual model has been presented. This model as been developed using multibody dynamics techniques suitable to describe the kinematic pairs between bones in a simplified way. In order to model physical joints an anatomical study has been carried out.

An ergonomic index involving joint physical limits has been also defined. The minimization of this index gives the extra equations required to bind the number of solutions.

In order to study inverse dynamic problems, 24 muscles have been added to the upper limb model. They have been described using the Zajac model modified by the authors in order to improve the computational efficiency. Moreover, an optimization

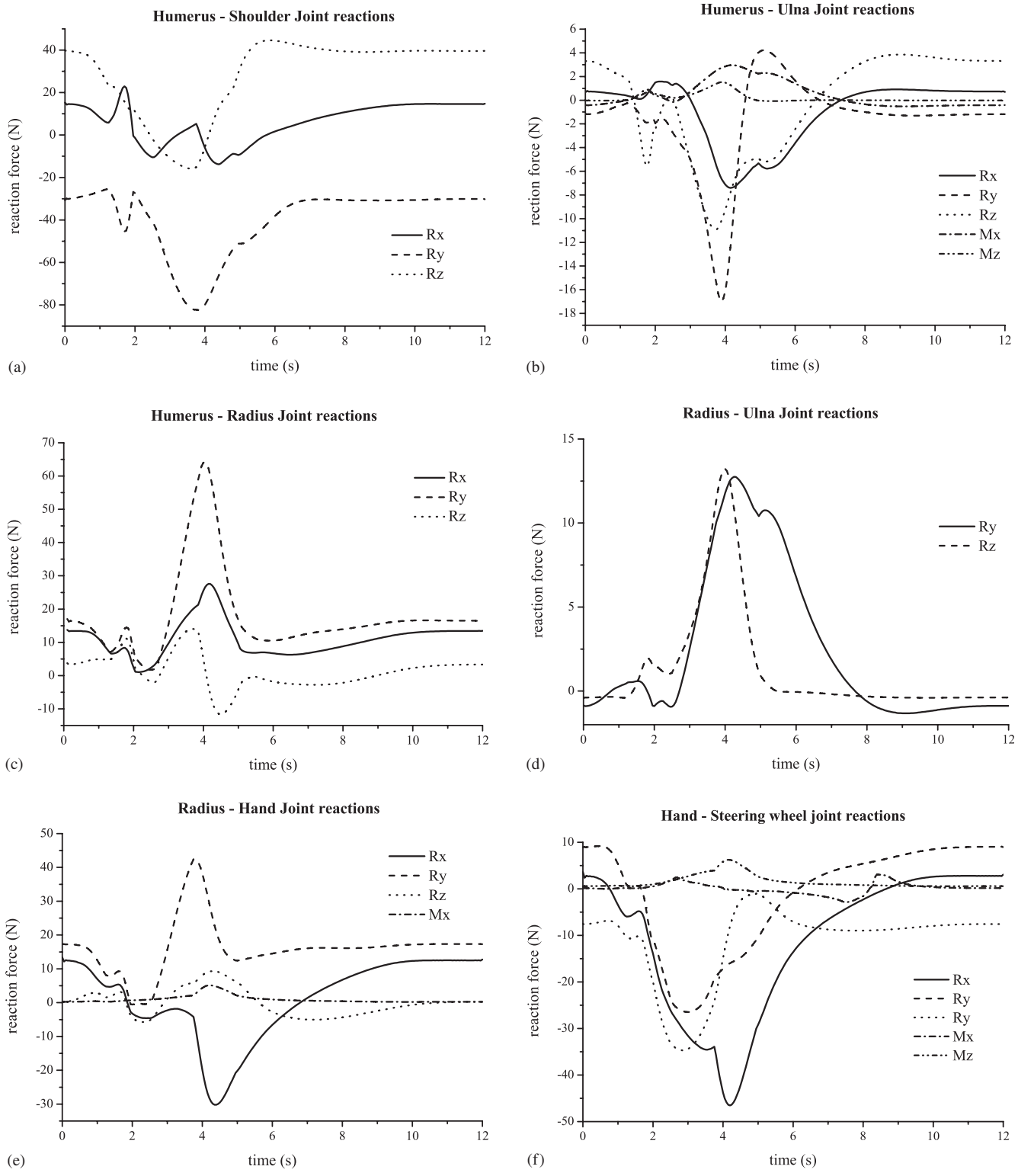

Fig. 7. Joint reaction forces and torques (values of forces are in N, values of torques are in Nm).

problem has been defined to solve the problem of muscular activations, which is described by a redundant system of equations. The model has been validated using results from literature and with collected experimental data for the movement of turn of a steering wheel. The present study is part of an investigation on the optimization of vehicle interior for less able car drivers. The knowledge of residual forces required for a safe

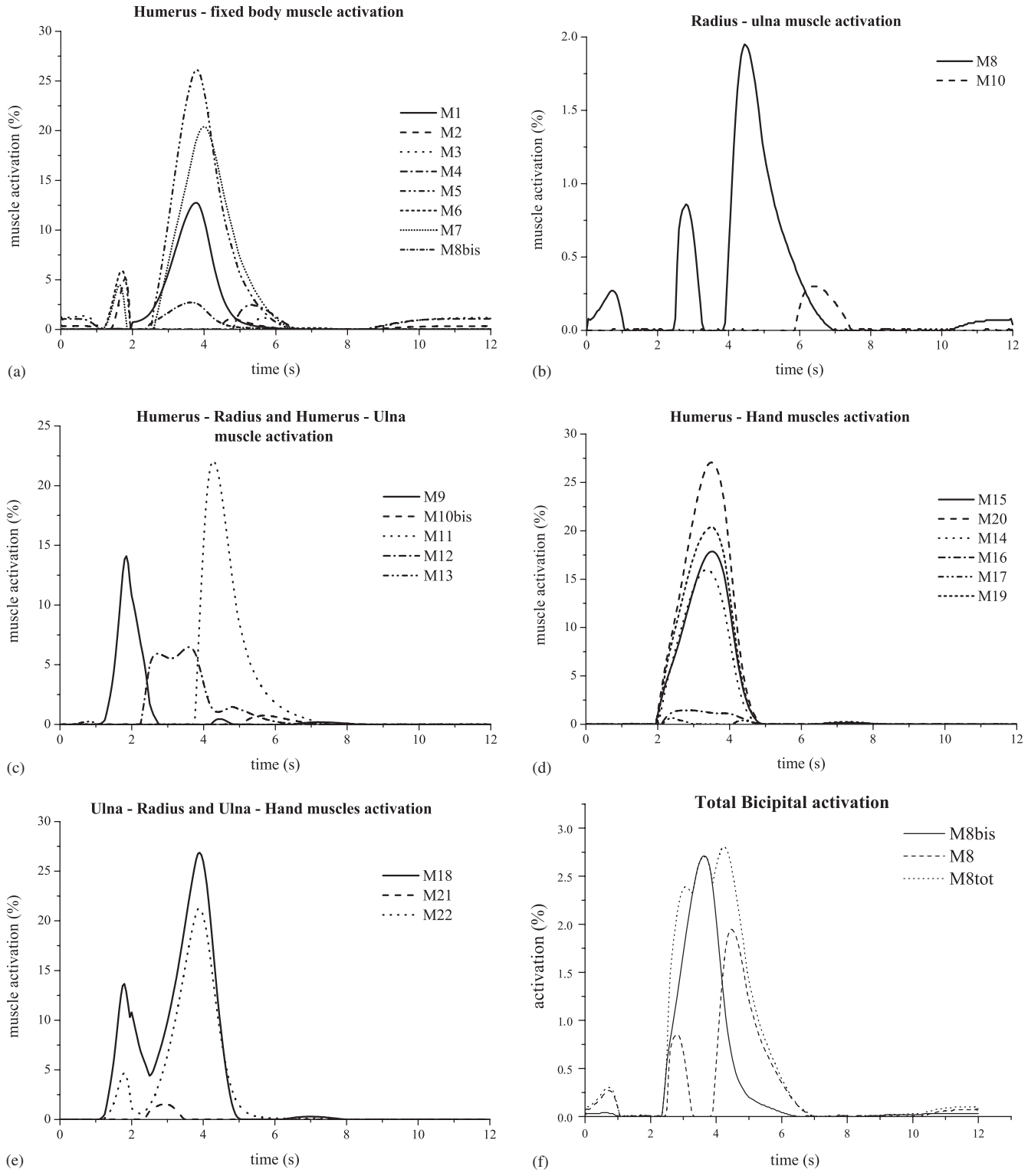

Fig. 8. Muscle activation percentages (for muscle definition see Table 2).

steering operation can be assessed in an objective way using the procedure herein proposed.

The model presented can mimic the behaviour of an upper limb. It has been successfully adopted for both ergonomic studies and dynamic simulation in order to predict muscular activations and joint reactions. The model has been experimentally validated measuring EMG signals during experimental tests on a car

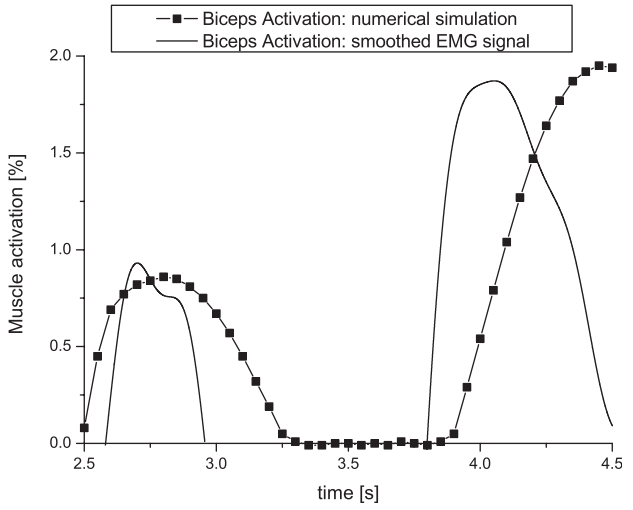

Fig. 9. Comparison between numerical and experimental activation patterns of biceps.

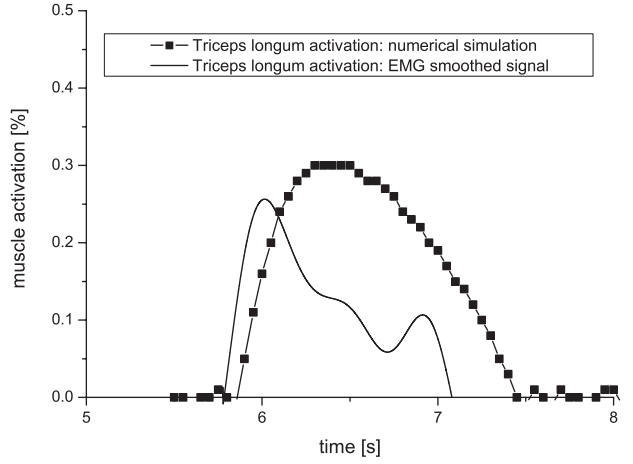

Fig. 10. Comparison between numerical and experimental activation patterns of triceps.

simulator. By comparing numerical results with the EMG signals one can conclude that the proposed model:

- approximates correctly the activation patterns;
- smooths the muscular activation peaks;
- simulates the right activation sequence and their maximum values.

Acknowledgement

The authors wish to acknowledge Dott. Ing. Luigi Bianchi of University of Rome Tor Vergata—Neurosciences Department, for his cooperation and technical support during EMG experimental tests.

References

Allard, P., Stokes, I., Blanchi, J.P., 1995. Three-dimensional analysis of human movement. Human Kinetics–Leeds.

Epstein, M., Hertzog, W., 1998. Theoretical Models of Skeletal Muscle. Wiley, England.

Garner, B.A., Pandy, M.G., 2003. Estimation of musculotendon properties in the human upper limb. Annals of Biomechanical Engineering 31, 207–220.

Kapandji, I.A., 1996. Joint Physiology 1. The Upper Limb. Maloine, Paris.

Kecskeméthy, A., Weinberg, A., 2005. An improved elasto-kinematic model of the human forearm for biofidelic medical diagnosis. Multibody System Dynamics 14, 1–21.

Kole, G.K., Vane den Bogert, A.J., Herzog, W., Gerritsen, K.G.M., 1996. Modelling of force production in skeletal muscle undergoing stretch. Journal of Biomechanics 29 (11).

Murray, W.M., Buchananan, T.S., Delp, S.L., 2000. The isometric functional capacity of muscles that cross the elbow. Journal of Biomechanics 33 (2).

Pigeon, P., Yahia, L.H., Feldman, A.G., 1996. Moment arms and lengths to human upper limb muscles as function of joint angles. Journal of Biomechanics 29 (10).

Rasmussen, J., Damsgaard, M., Christensen, S.T., de Zee, M., 2005a. Challenges In Musculoskeletal Modeling For Clinical Use. XXth Congress of the International Society of Biomechanics. Cleveland, Ohio, USA.

Rasmussen, J., de Zee, M., Damsgaard, M., Christensen, S.T., Marek, C., Siebertz K., 2005b. A General Method for Scaling Musculo-Skeletal Models. International Symposium on Computer Simulation in Biomechanics, Cleveland, Ohio, USA.

Rehbinder, H., Martin, C., 2001. A control theoretic model of the forearm. Journal of Biomechanics 34 (1).

Silva, M.P.T., 2004. Human motion analysis using multibody dynamics and optimization tools. Doctoral dissertation at Istituto Superior Tecnico–Lisboa.

Tal'Nov, A.N., Serenko, S.G., Strafun, S.S., Kostyukov, A.I., 1999. Analysis of the electromyographic activity of human elbow joint muscles during slow linear flexion movements in isotorque conditions. Neuroscience 90 (3), 1123–1136.

Valentini, P.P., Vita, L., 2003. David—A Multibody Virtual Dummy For Vibrational Comfort Analysis Of Car Occupants. Virtual Nonlinear Multibody Systems, NATO Science Series. Kluwer Academic Publishers, Dordrecht, The Netherlands.

Van der Helm, F.C.T., Veeger, H.E.J., 1996. Quasi static analysis of the muscle forces in the shoulder mechanism during wheelchair propulsion. Journal of Biomechanics 29 (1).

Veeger, H.E.J., Yu, B., An, K.N., Rozendal, R.H., 1997. Parameters for modelling the upper extremity. Journal of Biomechanics 30 (6).

Yamaguchi, G.T., 2001. Dynamic Modelling of Muscle-skeletal Motion. Kluwer Academic Publisher, Boston.

Yamazaki, Y., Itoh, H., Ohkuwa, T., 1995. Muscle activation in the elbow–forearm complex during rapid elbow extension. Brain Research Bulletin 38 (3), 285–295.

Zajac, F.E., 1989. Muscle and tendon: properties, models, scaling and applications to biomechanics and motor control. Critical Reviews in Biomechanical Engineering.

Zatsiorsky, V.M., 1995. Kinematics of human motion. Human Kinetics–Leeds.